JACC: ASIA VOL. 3, NO. 1, 2023

STATE-OF-THE-ART REVIEW

Advances in Diagnosis, Therapy, and Prognosis of Coronary Artery Disease Powered by Deep Learning Algorithms

Miao Chu, PhD,[a,*] Peng Wu, BSc,[a,*] Guanyu Li, BSc,[a,b] Wei Yang, PhD,[c] Juan Luis Gutiérrez-Chico, MD, PhD,[d] Shengxian Tu, PhD[a]

ABSTRACT

Percutaneous coronary intervention has been a standard treatment strategy for patients with coronary artery disease with continuous ebullient progress in technology and techniques. The application of artificial intelligence and deep learning in particular is currently boosting the development of interventional solutions, improving the efficiency and objectivity of diagnosis and treatment. The ever-growing amount of data and computing power together with cutting-edge algorithms pave the way for the integration of deep learning into clinical practice, which has revolutionized the interventional workflow in imaging processing, interpretation, and navigation. This review discusses the development of deep learning algorithms and their corresponding evaluation metrics together with their clinical applications. Advanced deep learning algorithms create new opportunities for precise diagnosis and tailored treatment with a high degree of automation, reduced radiation, and enhanced risk stratification. Generalization, interpretability, and regulatory issues are remaining challenges that need to be addressed through joint efforts from multidisciplinary community. (JACC: Asia 2023;3:1–14) © 2023 The Authors. Published by Elsevier on behalf of the American College of Cardiology Foundation. This is an open access article under the CC BY-NC-ND license (http://creativecommons.org/licenses/by-nc-nd/4.0/).

Coronary artery disease (CAD) remains the leading cause of mortality in the developed world, posing a challenge for global health policies. The prognosis and outcomes of percutaneous coronary intervention (PCI) for patients with CAD have significantly improved over the last decades because of the remarkable progress in technology and techniques. For example, artificial intelligence (AI), especially the deep learning (DL) subfield, is rapidly evolving and changing the landscape for the cardiology community, creating new opportunities to improve multiple aspects of the interventional workflow. The widespread DL technology has been powered by the rapidly growing amount of data, most prominently in some modalities of cardiovascular imaging. We aim to summarize the development and applications of different DL technologies for clinicians, interventionalists, and investigators with a particular focus on cardiovascular imaging-guided PCI. A brief review of algorithmic evolution and common computational imaging tasks provides the reader with the basis to understand DL technology. Challenges and future prospects for the clinical adoption of DL models are also discussed.

From the [a]Biomedical Instrument Institute, School of Biomedical Engineering, Shanghai Jiao Tong University, Shanghai, China; [b]Department of Cardiology, Aarhus University Hospital, Aarhus, Denmark; [c]School of Biomedical Engineering, Southern Medical University, Guangzhou, Guangdong, China; and [d]Bundeswehrzentralkrankenhaus (Federal Army Central Military Hospital), Koblenz, Germany. *Drs Chu and Wu contributed equally to this paper.

The authors attest they are in compliance with human studies committees and animal welfare regulations of the authors' institutions and Food and Drug Administration guidelines, including patient consent where appropriate. For more information, visit the Author Center.

Manuscript received October 18, 2022; revised manuscript received November 29, 2022, accepted December 1, 2022.

ISSN 2772-3747 https://doi.org/10.1016/j.jacasi.2022.12.005

ABBREVIATIONS AND ACRONYMS

CAD = coronary artery disease

CCTA = coronary computed tomography angiography

CMRA = coronary magnetic resonance angiography

CNN = convolutional neural network

DL = deep learning

FFR = fractional flow reserve

IVUS = intravascular ultrasound

OCT = optical coherence tomography

PCI = percutaneous coronary intervention

DEVELOPMENT OF DL NETWORKS

DL models consist of numerous artificial neural layers with parameters to be trained, nonlinearly transforming the input into output with no need of understanding the underlying mechanisms or the laws of biophysics. A typical pipeline for developing a DL model involves training, validation, and testing phases (**Figure 1**). During the training phase, the model learns parameters to efficiently perform its task using a specific data set dubbed the training data set. During the validation phase, the model fine-tunes hyperparameters related to the training strategy (eg, the learning rate and the numbers of hidden layers), which are critical for the model performance, using a different data set, namely the validation data set. Finally, the testing phase evaluates the objective and unbiased performance of the model on an independent data set (ie, the testing data set). The overlapping between the training, validation, and testing data sets during these 3 phases should be strictly avoided to prevent data leakage and overfitting in order to improve the generalizability of the models. Cost function reflects the discrepancy between the output predicted by the DL model and the ground truth provided by human experts. The minimization of the cost function through the back propagation algorithm[1] guides the model to iteratively learn the optimal parameters of neural layers during the training phase. Evaluation metrics are used for tuning hyperparameters (eg, learning rate) during the validation phase and for reporting the final performance of the model in the testing phase. Different models have been proposed to adapt to different tasks; in this paper, we introduce some milestones in the development of DL models in chronological order (**Figure 2**).

Inspired by the neuron connection in the human brain, the origins of the feedforward neural network (FNN) can be tracked back to 1943.[2] The architecture of the FNN consists of successively stacked layers, namely the input layer, output layer, and multiple hidden layers in between. Each layer contains multiple paralleled neurons that are connected to neurons in adjacent layers, passing the current value in a feedforward way. To deal with sequential data and image data, the recurrent neural network (RNN) and convolutional neural network (CNN) were proposed. The RNN was designed with feedback loops such that the current neuron state was dependent not only on the current input but also previous states.[3,4] The CNN was proposed by LeCun et al[5] in the 1990s; convolutional kernels with a fixed size and learnable parameters were used to scan the whole image as a sliding window to extract image features. The advantages of the CNN over the FNN, including shared parameters and less computational cost, have promoted the dominant position of the CNN in the DL field. The graph neural network (GNN) can be regarded as a generalization of the CNN from processing gridded data to unordered data,[6] such as a molecule structure in which the intrinsic intersample relationship should be preserved. Goodfellow et al[7] proposed the generative adversarial network (GAN) in 2014 by designing a pair of networks (ie, the generator and the discriminator) that are optimized by competing with each other, leading to a dynamic balance by the end of training. The Transformer is an attention-based DL model that was designed to handle sequential data by Google Brain in 2017.[8] The strength of the Transformer over other DL models lies in extracting long-distance dependencies of sequential data through a self-attention mechanism. Dosovitskiy et al adapted the Transformer to the image field by proposing the vision Transformer.[9] Afterward, other models, such as the Swin Transformer,[10] were proposed to address the high computational complexity and large-scale data requirements; they showed superior performance in various tasks.[10-13]

COMPUTATIONAL TASKS

The application of a DL model in coronary imaging can be roughly classified into 5 computational tasks: classification, segmentation, detection, reconstruction, and regression (**Figure 3**). The performance of DL models is evaluated by different metrics whose selection is dependent on the specific task. Details of the different metric formulas are available in Supplemental Table 1.

CLASSIFICATION. Image classification refers to assigning a certain label to the whole image according to the target object in the image. Numerous clinical scenarios could be formulated as a task of classification (eg, the diagnosis and prognosis of CAD, the phenotype of coronary plaque, and so on). Output labels could be dichotomous (eg, "normal/abnormal") or multicategory (eg, lipidic pool/calcium/fibrous tissue). Pretraining DL models on large-scale data sets and then fine-tuning them with domain-specific data is an effective solution to improve model performance. Accuracy is the most widely used metric to evaluate the performance of classification models. However, it may be biased for tasks with imbalanced

FIGURE 1 **The Pipeline of Developing a Deep Learning Model**

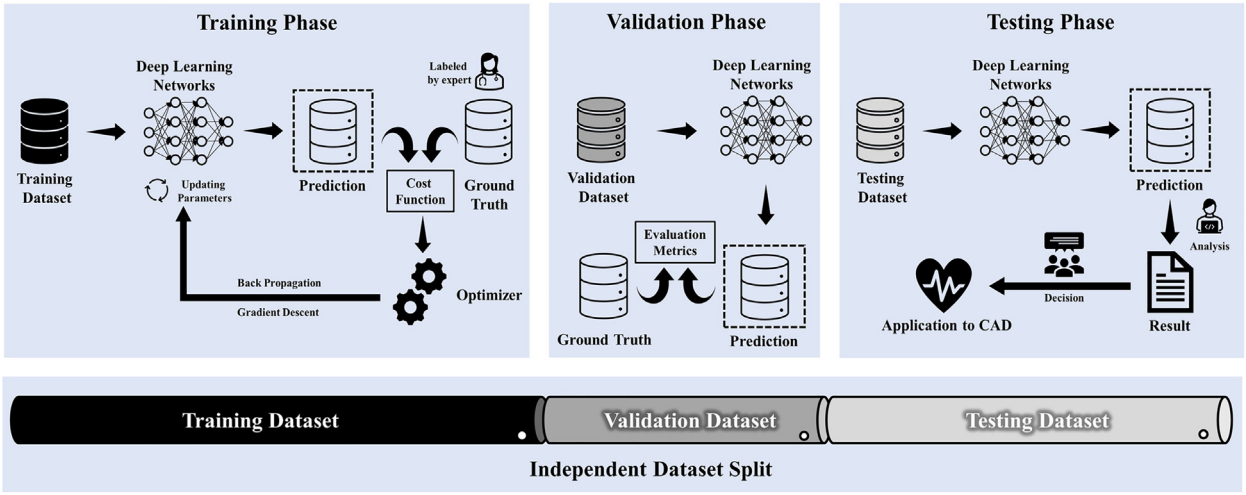

The pipeline includes training, validation, and testing phases using independent nonoverlapping data sets. The training phase optimizes model parameters by minimizing the cost function, the validation phase tunes the hyperparameters related to training strategy, and the testing phase evaluates the performance of the final model. The overlapping of the data used in the 3 phases should be strictly avoided. CAD = coronary artery disease.

data. The area under the receiver-operating characteristic curve is often used to evaluate the overall performance along with sensitivity, specificity, and positive/negative predictive values.

SEGMENTATION. Semantic segmentation could be considered as a dense classification in which each pixel or voxel in a 2-dimensional (2D) or 3-dimensional (3D) image, respectively, is classified into a label. The segmentation of arteries, plaques, and stents is a common task for coronary imaging. A CNN model with encoder-decoder architecture remains the first choice for segmentation tasks, with U-Net[14] and its variants being widely adopted. The encoder extracts imaging features that convert the input image into low-resolution feature maps, whereas the decoder projects learned features onto the original images with a dense prediction for each pixel. The segmentation performance is mostly evaluated by the metrics of Dice and Jaccard, which reflect the regional overlap between the model prediction and the ground truth. In addition, boundary distances between the prediction and the ground truth are quantified by metrics like the Hausdorff distance and the mean surface distance.

DETECTION. The detection task identifies a target object by outputting a bounding box enclosing it.[15,16] The detection of stenosis and plaques are paradigmatic applications in coronary imaging. Overall, detection models can be classified as anchor-based or anchor-free approaches. The anchor-based methods, such as the R-CNN series[17-20] and the YOLO series,[21,22] generate multiple anchors as candidates, and those containing objects with the highest confidence and largest overlapping area between the ground truth and the bounding box are selected. The anchor-free methods find the center of each object and infer its size to generate the bounding box. To evaluate the detection performance, object-level metrics like precision, recall, and the F1 score can be computed. The precision-recall curve is also plotted to report the average accuracy of the model.

RECONSTRUCTION. In general, image reconstruction refers to the construction of a target domain image from source domain signals, which could be divided into raw-to-image and postprocessing applications. The first one constructs the image from raw data collected by sensors, whereas the second one reconstructs the image from extracted features in source domain images. GAN models like the Cycle GAN[23] are commonly exploited for the reconstruction task. The quality of the reconstructed image can be evaluated by the following metrics: the mean absolute error, the mean square error, and their corresponding normalized items. Furthermore, structure similarity[24] and peak signal-to-noise ratio are also used.

REGRESSION. Regression is similar to classification in model structures, but the output of a regression

FIGURE 2 The Development of DL Model Architecture in Chronological Order

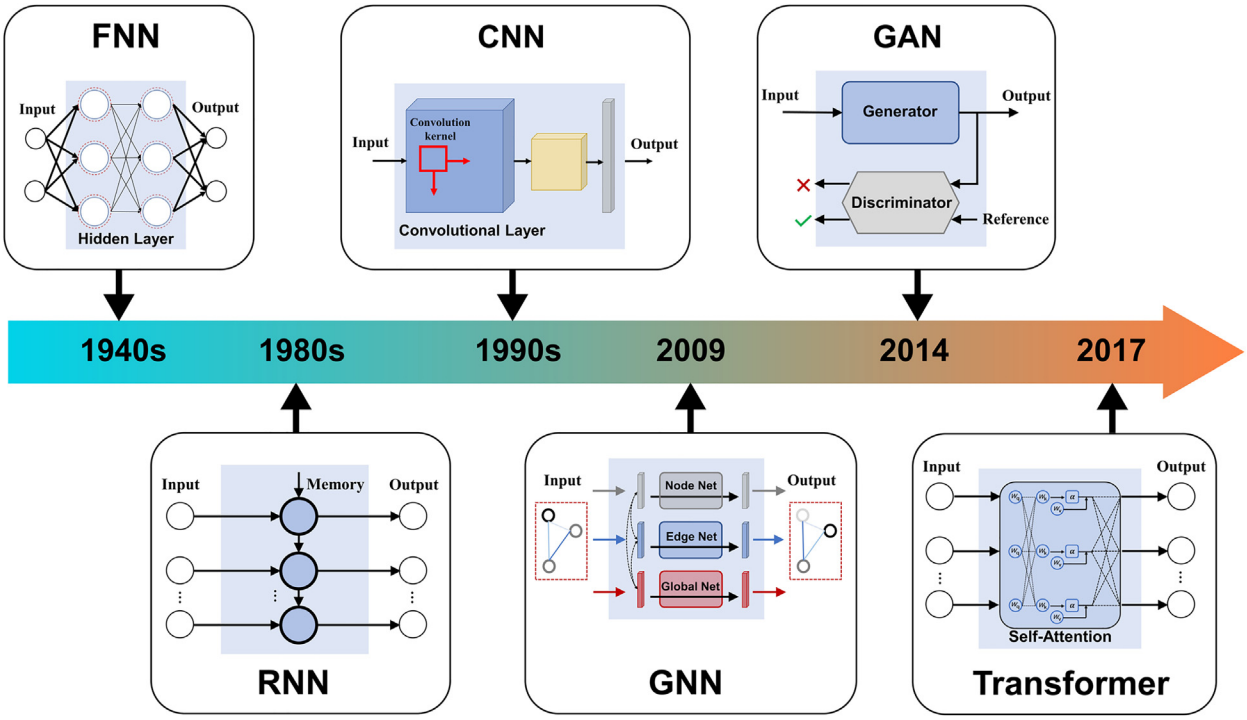

Milestones in the development of deep learning (DL) models include the feedforward neural network (FNN), recurrent neural network (RNN), convolutional neural network (CNN), graph neural network (GNN), generative adversarial network (GAN), and Transformer.

model is a continuous real number rather than a discrete integer. Anatomy or physiology indexes (eg, diameter stenosis, calcium score, and fractional flow reserve [FFR]) can be predicted from coronary imaging by well-designed regression models. Also, image registration within or across modalities could also be considered as a regression task of predicting deformation fields. The performance of a regression model is usually assessed by the difference between the predicted and the reference values through the mean absolute error and the mean square error. Furthermore, tests of agreement (eg, Bland-Altman, intraclass correlation coefficient, Lin's coefficient, and so on) and Pearson correlation are also reported to reflect the relationship between the predicted value and the ground truth.

CLINICAL APPLICATIONS

The clinical applications of DL are rapidly evolving and changing the landscape of the cardiology community, creating new opportunities to improve multiple aspects of the interventional workflow. We summarized these applications in line with the workflow of imaging-guided coronary intervention in the catheter lab (**Central Illustration**) involving image acquisition, diagnosis and risk stratification, interventional navigation, and therapy evaluation and optimization.

IMAGE ACQUISITION. As listed in **Table 1**, the application of DL to image reconstruction enables novel acquisition strategies, improving imaging quality while reducing artifacts and the radiation dose, as exemplified in coronary magnetic resonance angiography (CMRA). Free-breathing whole-heart 3D CMRA allows for the visualization of coronary arteries, but it requires a prohibitively long scan time. To overcome this limitation, undersampling techniques paralleled by advanced reconstruction algorithms have been proposed. For instance, Küstner et al[25] developed and evaluated a generative adversarial super-resolution network that enabled 16-fold resolution upsampling and reconstruction of free-breathing 3D CMRA in less than a 1-minute scan time, thus significantly boosting the acquisition speed. This supervised DL model was trained and tested on 47 and 15 patients, respectively. Improved vessel sharpness compared with low-resolution CMRA was reported.

FIGURE 3 **Typical Computational Tasks of DL Models With Corresponding Evaluation Metrics**

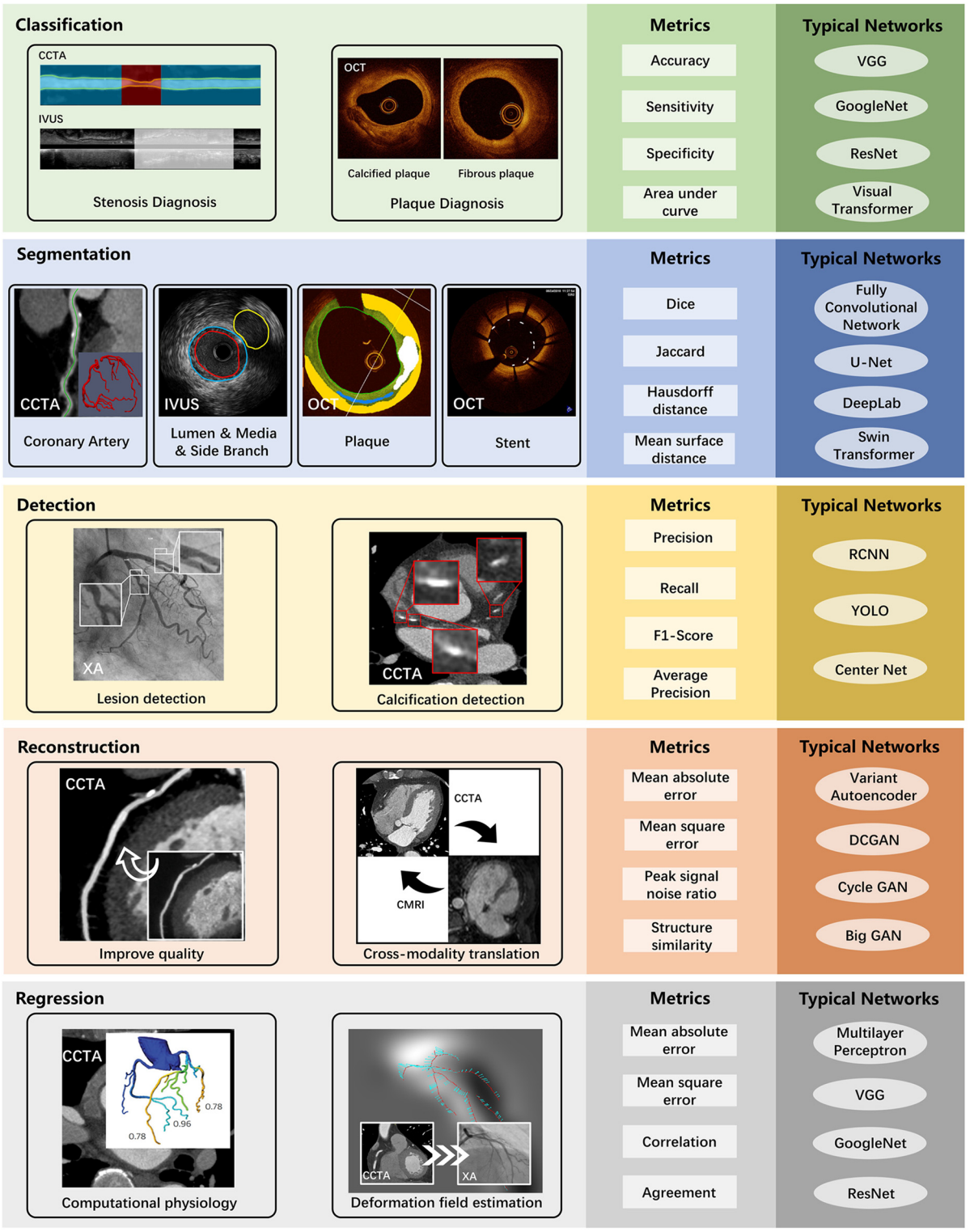

Typical computational tasks include classification, segmentation, detection, reconstruction, and regression. CCTA = coronary computed tomography angiography; CMRA = coronary magnetic resonance angiography; DCGAN = deep convolutional generative adversarial network; DL = deep learning; GAN = generative adversarial network; IVUS = intravascular ultrasound; OCT = optical coherence tomography; RCNN = region-based convolutional neural network; VGG = visual geometry group; XA = X-ray angiography.

CENTRAL ILLUSTRATION **Clinical Applications of Deep Learning in the Workflow of Interventional Catheterization**

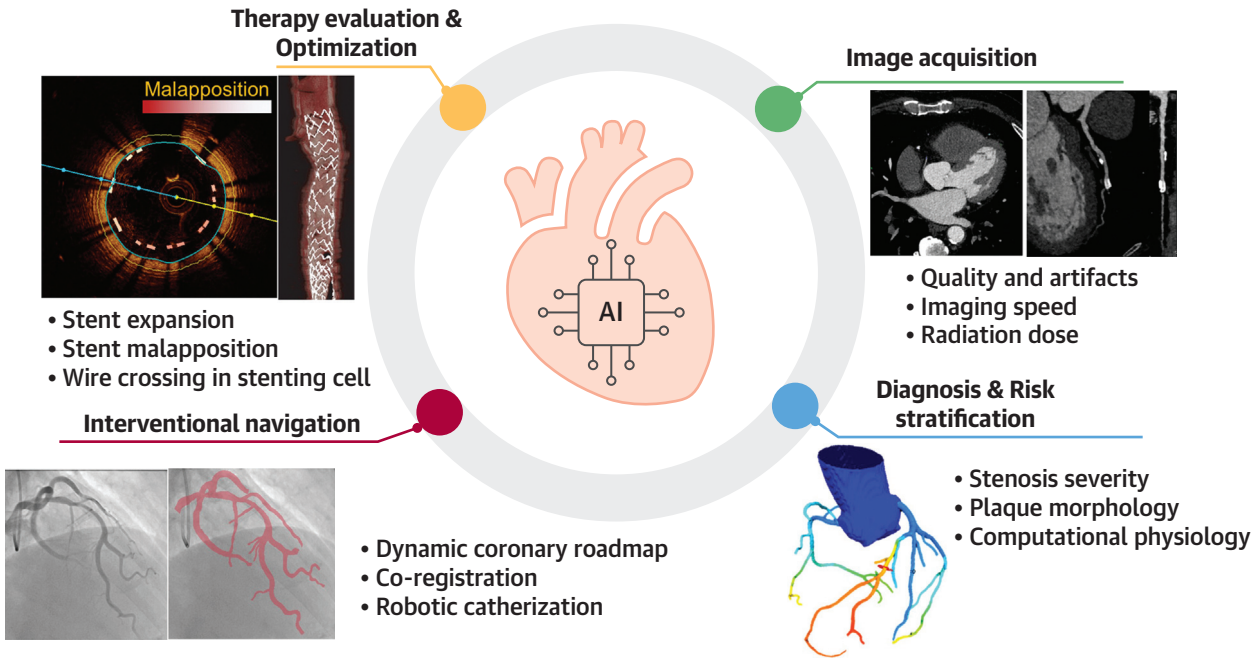

Chu M, et al. JACC: Asia. 2023;3(1):1-14.

Deep learning models open new opportunities to improve multiple aspects of the interventional workflow, involving image acquisition, diagnosis and risk stratification, interventional navigation, and therapy evaluation and optimization. AI = artificial intelligence.

DL models have also been applied to coronary computed tomography angiography (CCTA) reconstruction.[26,27] Chen et al[28] developed DL technology to reconstruct high-quality computed tomographic images by training models using a low-dose sinogram and paired high-quality CCTA images as ground truths. Clinical studies have confirmed that DL-powered CCTA reconstruction resulted in the reduction of the radiation dose and improved image quality without compromising stenosis or plaque assessment.[29,30]

Finally, novel reconstruction procedures also have been applied to intravascular imaging, especially to intravascular ultrasound (IVUS), for the correction of cardiac motion artifacts.[31] The majority of commercial IVUS systems do not take the phase of the cardiac cycle into account during reconstruction, resulting in inconsistent alignment and jagged lumen contour in the longitudinal view. Stevens et al[32] proposed a DL reinforcement framework to efficiently extract information from the acoustic scene in which the sampling of the current frame is conditioned on the reconstruction of the previous frame. Analysis of end-diastolic-gated IVUS frames was reported to be superior to the conventional nongated IVUS in terms of measurement reproducibility.[33]

DISEASE DIAGNOSIS AND RISK STRATIFICATION. Accurate diagnosis and enhanced risk stratification are instrumental for appropriate decision making and tailored treatment of CAD, with tasks like coronary stenosis quantification, plaque characterization, and physiology assessment as cornerstones (Table 2). DL models have proven excellent performance in the diagnosis of stenosis using dedicated CNN architectures, such as the cutting-edge feature extraction network and the spatiotemporal attention module.[34] Du et al[35] trained 2 DL models for the identification of coronary artery segments and the recognition of lesion morphology, respectively, using a large data set of over 20,000 angiograms. The models achieved an accuracy of 98.4% in vessel segment recognition and an F1 score of 0.829 for stenotic lesion detection. The prognostic relevance of plaque characterization for the prediction of future coronary events in high-risk patients has been consistently reported in different studies using different imaging modalities.[36-38] DL models have been widely used to assess plaques on CCTA. For example, in a recent

TABLE 1 Applications of DL Models in Coronary Image Acquisition

First Author (Ref. #)	Clinical Application	Modality	Computational Task	Network	Computational Performance	Clinical Performance	Year
Fuin et al[75]	Acceleration	CMRA	Reconstruction	CNN	–	Acquisition time: ~2.5 min	2020
Qi et al[76]	Acceleration	CMRA	Reconstruction	CNN FNN	PSNR: 27.86 ± 3.00 dB SSIM: 0.78 ± 0.06	Acquisition time: ~2.5 min	2021
Küstner et al[25]	Acceleration	CMRA	Reconstruction	CNN GAN	–	Acquisition time: < 1 min	2021
Benz et al[29]	Reduced radiation	CCTA	Reconstruction	CNN	–	Dose: 0.8 mSv	2022
Tatsugami et al[27]	Reduced radiation	CCTA	Reconstruction	CNN	–	Dose: 5.4 mSv	2019
Azizmohammadi et al[77]	Reduced radiation	XA	Reconstruction	CNN RNN	SSIM: 0.82	Dose reduction, %: 30	2022
Jung et al[78]	Artifact correction	CCTA	Reconstruction	CNN	PSNR: 33.6 dB SSIM: 0.97	–	2020
Deng et al[79]	Artifact correction	CCTA	Reconstruction	CNN GAN	PSNR: 24.96 dB SSIM: 0.769 NMSE: 0.031	–	2022
Xia et al[80]	Artifact correction	IVUS	Regression	CNN GAN	SNR: 114.76 dB	–	2022
Bajaj et al[81]	Artifact correction	IVUS	Classification	RNN FNN	Accuracy, %: 80.4	Mean difference with electrocardiogram: 3 ± 112 ms	2021

CCTA = coronary computed tomography angiography; CMRA = coronary magnetic resonance angiography; CNN = convolutional neural network; DL = deep learning; FNN = feedforward neural network; GAN = generative adversarial network; GNN = graph neural network; IVUS = intravascular ultrasound; NMSE = normalized mean square error; OCT = optical coherence tomography; PSNR = peak signal-to-noise ration; RNN = recurrent neural network; SNR = signal-to-noise ratio; SSIM = structure similarity; XA = X-ray angiography.

international multicenter study, a DL system was developed for rapid and automated quantification of plaque volume on CCTA, resulting in excellent agreement with IVUS (intraclass coefficient = 0.949) at a much higher speed of CCTA analysis than expert analysts (5.65 ± 1.87 min/patient vs 25.66 ± 6.79 min/patient).[39] Lin et al[39] developed and validated DL-enabled plaque and stenosis quantification from CCTA, which proved prognostic value in predicting the risk of future myocardial infarction in a large cohort of patients with stable chest pain. The integration of the parameters of plaque quantification could also enhance the predictive value of the currently established risk stratification models.[40,41] Furthermore, novel imaging predictors of prognosis have been extracted from CCTA by analyzing the radiomic profile of epicardial adipose tissue, which was capable of capturing permanent structural changes in perivascular adipose tissue and significantly improving risk prediction for adverse coronary events.[42,43] This might be a paramount leap forward to further expand large-scale applications of CCTA as a first-line diagnostic tool for the screening of CAD.[44,45] This trend entails the use of CCTA in large populations as a default screening test; therefore, DL-driven improvements in the workflow of CCTA will have a huge impact on health systems. Nevertheless, CCTA is inherently limited for detailed plaque characterization as required in clinical practice for precise risk stratification or for planning of the interventional strategy. For advanced plaque characterization, invasive imaging remains the gold standard.[46]

Chu et al[47] developed a deep CNN model for comprehensive plaque characterization in optical coherence tomography (OCT), which was trained on a large data set of over 500 OCT pull backs from multiple centers. The model was validated against expert consensus from 3 internationally renowned core labs in an external cohort, achieving the best diagnostic accuracy with fibrous plaques (97.6%) followed by lipidic plaque (90.5%) and calcifications (88.5%) and thus enabling the characterization of coronary plaques in a fully automated and timely efficient way. A novel plaque vulnerability index named the lipid-to-cap ratio was recently proposed on the basis of this DL-enabled automatic plaque segmentation,[48] integrating the 2 most critical morphologic features of plaque to determine its vulnerability: lipidic plaque burden and cap thickness. The lipid-to-cap ratio was superior to classical morphologic parameters, such as the minimal lumen area, plaque burden, or thin-cap fibroatheroma, in predicting nonculprit vessel-related major adverse cardiovascular events at a 2-year follow-up.[48]

Physiology-guided revascularization has consistently proven better clinical outcomes than traditional angiographic guidance in multiple clinical scenarios; therefore, it has been granted a Class I indication in the current guidelines for myocardial revascularization in stable CAD.[49] FFR is regarded as the gold standard for coronary physiology assessment

TABLE 2 Applications of DL Models in Diagnosis and Risk Stratification of Coronary Artery Disease

First Author (Ref. #)	Clinical Application	Modality	Computational Task Network	Network	Computational Performance	Clinical Performance	Year
Du et al[35]	Lesion Diagnosis	XA	Detection	CNN GAN	F1 score: stenosis 0.829 Total occlusion: 0.810 Calcification: 0.802 Thrombosis: 0.823 Dissection: 0.854	AUC: stenosis 0.801 Total occlusion 0.759 Calcification 0.799 Thrombosis 0.778 Dissection 0.863	2021
Zhao et al[82]	Stenosis Diagnosis	XA	Segmentation	CNN	Dice: 0.89	True positive rate: 0.68	2021
Pang et al[83]	Stenosis Diagnosis	XA	Detection	CNN	Precision: 0.949 F1 score: 0.881	–	2021
Li et al[84]	Stenosis Diagnosis	CCTA	Segmentation	CNN	Dice: 0.771 ± 0.021	AUC: 0.737	2022
Ma et al[85]	Stenosis Diagnosis	CCTA	Classification	CNN Transformer	Accuracy: 0.92 Specificity: 0.96	Correlation: $r = 0.74$	2021
Tu et al[60]	FFR computation	XA	Segmentation	CNN	–	Correlation: $r = 0.90$ Agreement: 0.00 ± 0.05 AUC: 0.97	2021
Wang et al[86]	FFR computation	CCTA	Regression	RNN FNN	–	Correlation: $r = 0.683$ Agreement: −0.17 to 0.16 AUC: 0.933	2019
Kumamaru et al[87]	FFR computation	CCTA	Regression	CNN GAN FNN	–	AUC: 0.78	2020
Yu et al[63]	FFR computation	IVUS	Segmentation	CNN GAN	–	Correlation: $r = 0.87$ Agreement: −0.02 ± 0.08 AUC: 0.97	2021
Zreik et al[88]	Plaque Identification	CCTA	Classification	CNN FNN RNN	Accuracy: 0.77	/	2019
Wolterink et al[89]	Calcium Scoring	CCTA	Segmentation	CNN	–	Correlation: $r = 0.94$ Agreement: −38.7 to 38.3	2016
Chu et al[47]	Plaque Characterization	OCT	Segmentation	CNN	Dice: fibrous 0.906 Lipidic: 0.772 Calcific: 0.848	Correlation: $r = 0.98$ Agreement, %: 0.35 ± 4.312	2021
Du et al[90]	Plaque Identification	IVUS	Segmentation	CNN	HD: lumen 0.336 mm Media 0.367 mm	Correlation: $r = 0.98$	2022
Jun et al[91]	TCFA Identification	IVUS	Segmentation	CNN FNN	–	AUC: 0.911	2019
Moon et al[92]	CAD Diagnosis	XA	Classification	CNN FNN	Accuracy: 0.943	AUC: 0.956	2021
Zreik et al[93]	CAD Diagnosis	CCTA	Segmentation	CNN FNN	Dice: 0.91	AUC: 0.74 ± 0.02	2018
Tamarappoo et al[94]	Predication of hard coronary event	CCTA	Segmentation	XG Boost	–	AUC: 0.81	2021
Commandeur et al[95]	Prediction of myocardial infraction and coronary death	CCTA	Classification	XG Boost	–	AUC: 0.82 HR: 10.38	2020
Kwan et al[96]	Prediction of revascularization	CCTA	Regression	–	–	AUC: 0.78	2021
Lin et al[39]	Prediction of cardiovascular risk	CCTA	Segmentation	CNN RNN	Dice: Vessel wall 0.94 Lumen and plaque: 0.90	HR: Plaque volume: 5.36 Diameter stenosis: 2.49	2022
Hong et al[48]	Risk stratification	OCT	Segmentation	CNN	–	AUC: 0.826 HR: 42.73	2022
Neleman et al[97]	Prediction of POCE	IVUS	Classification	SVM	–	HR: 1.51	2021

AUC = area under curve; CAD = coronary artery disease; FFR = fractional flow reserve; HD = Hausdorff distance; NPV = negative predictive value; POCE = patient-oriented composite endpoint; PPV = positive predictive value; TCFA = thin-cap fibroatheroma; other abbreviations as in Table 1.

and has generated a huge corpus of evidence over time.[50-52] However, the adoption of FFR in real-world surveys is low[53] because of several factors (eg, budgetary restrictions or the need to induce hyperemia). With the aim of overcoming these limitations, some FFR estimators have been developed and quickly gained popularity, such as resting indexes or computational physiology. These alternative

TABLE 3 Applications of DL Models in Interventional Navigation

First Author (Ref. #)	Clinical Application	Modality	Computational Task	Network	Computational Performance	Clinical Performance	Year
Wu et al[70]	Dynamic coronary roadmap	XA-CCTA	Regression	CNN	–	Mean projection distance: 1.13 ± 0.83 mm	2022
Ma et al[68]	Dynamic coronary roadmap	XA	Segmentation	CNN	–	Mean error: 1.29 ± 1.76 mm	2020
Jeone et al[69]	Dynamic coronary roadmap	XA	Reconstruction	CNN	PSNR: 34.09 ± 2.28 dB	Registration error: 1.06 ± 0.18 mm	2021
Fang et al[98]	Dynamic coronary roadmap	XA	Regression	CNN RNN	RMSE: 0.06-0.26	Correlation: 0.64-0.94	2020
Kweon et al[99]	Navigation	XA	Regression	CNN	–	Success rate, %: 2D phantoms 98 3D phantoms 99	2021
Sayadi et al[100]	Robotic PCI	–	Regression	FNN	MAE: 0.018 ± 0.012 N	Correlation: 0.99	2021

MAE = mean absolute error; PSNR = peak signal-to-noise ration; RMSE = root mean square error; other abbreviations as in Table 1.

methods have not only become popular but also generated compelling and consistent evidence[54-56] and even gained a Class I indication in the guidelines on par with FFR.[49] In this line, imaging-based computational physiology is an active area of research.[57] DL has been introduced to computational physiology either in the statistical method alone or combined with the mechanistic method. The statistical method is purely data driven in which predictions of hemodynamic significance (ie, FFR <0.80) or FFR values are directly obtained from coronary imaging through a classification or regression model. For example, Itu et al[58] trained a DL model using 28 geometric features extracted from CCTA as input and computational fluid dynamic simulation values as the ground truth, aiming at integrating complex nonlinear relationships between various anatomic features.[58] However, its correlation with invasive FFR was moderate ($r = 0.62$) in a multicenter cohort of 525 vessels from 351 patients.[59] Conversely, hybrid methods combining statistical models and the mechanistic theory of coronary blood flow outperformed purely data-driven models. For instance, Tu et al[60] developed a new method of FFR computation from a single X-ray angiographic view (ie, law-based quantitative flow ratio [μQFR]) powered by DL models for automatic delineation of the coronary arteries as geometry modeling as well as boundary conditions for simplified flow dynamics equations. μQFR showed excellent correlation and agreement with invasive FFR[60,61] and the 3D quantitative flow ratio.[62] Moreover, there are novel computational methods based on intravascular imaging of OCT and IVUS (ie, optical flow ratio [OFR] and ultrasonic flow ratio [UFR]) that allow morphofunctional evaluation within 1 single imaging pull back. OFR and UFR achieved excellent diagnostic accuracies (93% and 92%, respectively) to identify significant FFR.[63-65]

INTERVENTIONAL NAVIGATION. In addition to bringing benefits to CAD diagnosis and risk stratification, DL has also been applied to assist in PCI navigation with enhanced procedure efficiency and convenience (Table 3). One significant application is the dynamic coronary roadmap (DCR), which enables continuous visual feedback for cardiologists during intervention by superimposing coronary arteries onto a fluoroscopic image in a dynamic real-time fashion. Clinical studies based on a commercialized DCR system (Philips Healthcare) reported a significant reduction in contrast volume (22%) and fluoroscopy time (30%).[66,67] The first DCR system could be dated back to 1989; it was developed by Elion's group, and the application of DL greatly addressed the technical challenges of motion compensation caused by respiration and heartbeat. Ma et al[68] developed a CNN model to compensate respiratory-induced motion via a tracking catheter tip. A total of 55 patients were enrolled, and the proposed tracking model had a median and maximal error of 0.96 mm and 17.72 mm for testing images. The total average speed for the proposed DCR workflow is 66.7 ms/frame, showing potential in real-time application. However, the method requires manual annotation of the catheter tip off-line. More recently, a deep generative model was proposed for DCR by transforming registration into an image generation problem.[69] Coronary and respiratory motions were implicitly compensated by the GAN model, and it could be applied to arrhythmia patients with irregular electrocardiogram signals. In addition to extracting information from a single modality, coregistration of different imaging modalities usually adds valuable information, aiding in complicated interventions such as chronic total occlusion. For example, fusing a preprocedural CCTA image with angiography during intervention assists in procedural planning and guidewire manipulation.

TABLE 4 Applications of DL Models in Therapy Evaluation and Optimization

First Author (Ref. #)	Clinical Application	Modality	Computational Task	Network	Computational Performance	Clinical Performance	Year
Lu et al[101]	Stent evaluation	OCT	Detection	Bagged decision tree	Recall: uncovered 0.82 Covered 0.99	Correlation: stent area $r = 0.97$ Lumen area $r = 0.99$	2020
Wang et al[102]	Stent evaluation	OCT	Detection	Bayes Network	Precision: 0.84 Recall: 0.91	Correlation: stent area $r = 0.988$	2015
Wissel et al[103]	Stent evaluation	IVUS	Segmentation	CNN FNN	Dice: encoder (0.824) Decoder (0.611)	–	2021
Wu et al[71]	Stent evaluation and healing analysis	OCT	Segmentation	CNN	Dice: 0.907 Jaccard: 0.838	Correlation: minimum stent area $r = 0.952$ Malapposition distance $r = 0.983$ Coverage thickness $r = 0.987$	2020
Yang et al[104]	Stent evaluation and healing analysis	OCT	Detection	CNN	Precision: 0.932	Correlation: stent area $r = 0.918$-0.954	2021
Nam et al[105]	Stent evaluation and healing analysis	OCT	Segmentation	FNN	–	Correlation: protrusion distance $r > 0.99$ Neointimal thickness $r > 0.99$	2016
Lu et al[106]	Stent evaluation and healing analysis	OCT	Classification	Support vector machine	Sensitivity, %: 94 Specificity, %: 90	AUC: 0.97	2019
Min et al[73]	Stent apposition predication	IVUS	Classification	CNN FNN	PPV: 0.70 NPV: 0.96 Accuracy: 0.94	AUC: 0.94 Correlation: stent area $r = 0.802$	2021

AUC = area under the curve; NPV = negative predictive value; PPV = positive predictive value; other abbreviations as in Table 1.

It is a technique of 3D/2D medical image registration, which involves modality transformation across 3D/2D images and deformation field computation. Wu et al[70] developed a DL model named the CAR-Net for deformable 3D/2D coronary artery registration. An average registration error of the mean projection distance of 1.13 mm was achieved for the proposed method on the clinical testing data set. However, heavy preprocessing steps including vessel segmentation and centerline extractions were required. Further refinement of fusion algorithms is to be expected. Furthermore, advanced DL technology applied to robotic-assisted catheterization holds promise for complete automation.

THERAPY EVALUATION AND OPTIMIZATION. Intravascular imaging poststenting is indicated to evaluate the result after stent deployment and eventually detect suboptimal findings that need optimization. However, a frame-per-frame analysis of the whole pull back, or even the systematic analysis of selected frames at periodic intervals (eg, 1 mm), is cumbersome and time-consuming to be routinely applied in the catheterization laboratory for clinical decision making. Rapid and automatic quantification of stent expansion and apposition is instrumental to streamline the workflow of PCI optimization. Some DL models have been developed for stent segmentation and detection with this aim, as shown in Table 4. Wu et al[71] designed a CNN model with multiscale shortcut connections and pseudo-3D input to aggregate the information from adjacent OCT frames. The model was trained on over 10,000 cross-sectional images and was independently tested in more than 21,000 images from 170 OCT pull backs. Excellent segmentation (Dice = 0.907) and detection (Precision = 0.943) performances were achieved for different sources of images. In comparison with previous semiautomated methods, the DL model enabled real-time stent quantification at a speed of 0.02 seconds per cross-sectional image. Interestingly, the accurate stent detection enabled precise 3D rendering, which can facilitate a quick evaluation of the stent deployment at first glance, while being instrumental for other clinical applications, such as the wire crossing through the right stent cell, the identification of previously implanted stent types,[72] or the impact of cardiac motion artifact[31] (Central Illustration).

In addition to the evaluation of the stent result in postprocedural imaging, Min et al[73] developed a DL model to predict stent underexpansion from preprocedural IVUS. Semantic features of lesion morphology derived from a CNN model together with procedural information like stent diameter, inflation pressure, or balloon diameter were used for regression, aiming to predict the stent area and the subsequent classification of stent underexpansion. A significant correlation was observed between the predicted stent area from the preprocedural IVUS and the measured area in poststenting images ($r = 0.802$). By predicting a potential risk for underexpansion, the DL model provides critical information to guide plaque preparation tailored to the specific requirements of each lesion in escalating complexity,

from simple predilatation to the use of sophisticated systems of plaque debulking, thus maximizing the likelihood of procedural success and optimizing the result to warrant optimal clinical outcome after PCI.

FUTURE PROSPECTS

Although DL models show promising performance across all the spectrum of CAD diagnosis, treatment, and prognosis hitherto, there are still limitations of DL and unaddressed challenges ahead. First, DL models are vulnerable to adversarial inputs because they rely on statistical patterns of the data rather than understanding inputs in human sense. A shift of the data distribution from the training data set may lead to completely different output by DL models. Medical imaging varies among different vendors and acquisition strategies. Therefore, it raises a major concern on the generalization ability of DL models across different clinical scenarios. Another relevant issue is the interpretability and transparency. DL models are notorious for its inherent "black box" feature, especially for high-level intelligent tasks of risk stratification and prognosis prediction.[74] There is a lack of understanding of the models' behavior and decision-making process. The integration of prior knowledge, biophysical modeling, and mechanistic theory would be complementary to purely data-driven DL models and might help improve model generalizability and interpretability. Second, the model behavior is largely dependent on the fed adjudication (data annotation), which is usually obtained from experienced experts. Notarized data annotation in line with expert consensus is essential for producing an unbiased model. Of note, extensive data annotation used to be an obstacle for DL development; however, advanced algorithms such as data generation by GAN, novel training pipelines of unsupervised learning (ie, no annotation), semisupervised learning (ie, annotation for a subset of input), or weakly supervised learning (ie, simplified coarse annotation) have largely alleviated the dependency of manual data annotation. Finally, the majority of AI models are at the stage of proof of concept, awaiting prospective clinical trials from large cohorts of patients. The efficacy of the model should be validated against the current state-of-the-art clinical standards through well-designed trials. It is reassuring to notice that new guidelines from regulatory authorities have now been set in place to better standardize the rapid development of AI technology and its deployment in clinical practice.

HIGHLIGHTS

- DL creates opportunities to improve the interventional workflow in the cardiology community.
- Technology development and clinical applications of DL in the diagnosis and treatment of coronary artery disease are reviewed.
- The remaining challenges for DL include generalization, interpretability, and individual equity.

CONCLUSIONS

Advanced DL algorithms open new opportunities for precise diagnosis and tailored treatment in cardiology with a high degree of automation, reduced radiation, and enhanced risk stratification. Generalization, interpretability, and regulatory issues are remaining challenges that need to be addressed through joint efforts from multidisciplinary community.

FUNDING SUPPORT AND AUTHOR DISCLOSURES

This study was supported by the Natural Science Foundation of China (82020108015 and 81871460). Dr Tu reported research grants and consultancy from Pulse Medical. All other authors have reported that they have no relationships relevant to the contents of this paper to disclose.

ADDRESS FOR CORRESPONDENCE: Dr Shengxian Tu, Room 123, Med-X Research Institute, Shanghai Jiao Tong University, No. 1954, Hua Shan Road, Shanghai 200030, China. E-mail: sxtu@sjtu.edu.cn. Twitter: @ChuMiao_, @JuanLuisGutChic.

REFERENCES

1. Rumelhart DE, Hinton GE, Williams RJ. Learning representations by back-propagating errors. *Nature*. 1986;323:533-536.

2. McCulloch WS, Pitts W. A logical calculus of the ideas immanent in nervous activity. *Bull Math Biophys*. 1943;5:115-133.

3. Jordan MI. Serial order: a parallel distributed processing approach. *Adv Psychol*. 1997;121:471-495.

4. Elman JL. Finding structure in time. *Cogn Sci*. 1990;14:179-211.

5. LeCun Y, Bottou L, Bengio Y, Haffner P. Gradient-based learning applied to document recognition. *Proc IEEE*. 1998;86:2278-2324.

6. Scarselli F, Gori M, Tsoi AC, Hagenbuchner M, Monfardini G. The graph neural network model. *IEEE Trans Neural Netw*. 2008;20:61-80.

7. Goodfellow I, Pouget-Abadie J, Mirza M, et al. Generative adversarial nets. *Adv Neural Inf Process Syst*. 2014;27:2672–2680.

8. Vaswani A, Shazeer N, Parmar N, et al. Attention is all you need. *Adv Neural Inf Process Syst*. 2017;30:arXiv, 1706.03762.

9. Han K, Wang Y, Chen H, et al. A survey on vision transformer. *IEEE Trans Pattern Anal Mach Intell*. 2023;45(1):87–110. https://doi.org/10.1109/TPAMI.2022.3152247

10. Liu Z, Lin Y, Cao Y, et al. Swin transformer: hierarchical vision transformer using shifted windows. Paper presented at: Proceedings of the IEEE/CVF International Conference on Computer Vision; October 11, 2021-October 17, 2021; Montreal, Quebec, Canada.

11. Zheng S, Lu J, Zhao H, et al. Rethinking semantic segmentation from a sequence-to-sequence perspective with transformers. Paper presented at: Proceedings of the IEEE/CVF Conference on Computer Vision and Pattern Recognition; June 19, 2021-June 25, 2021; Nashville, TN.

12. Fang Y, Liao B, Wang X, et al. You only look at one sequence: rethinking transformer in vision through object detection. *Adv Neural Inf Process Syst*. 2021;34:26183–26197.

13. Tang Y, Yang D, Li W, et al. Self-supervised pre-training of Swin transformers for 3d medical image analysis. Paper presented at: Proceedings of the IEEE/CVF Conference on Computer Vision and Pattern Recognition; June 19, 2022-June 24, 2022; New Orleans, LA.

14. Ronneberger O, Fischer P, Brox T. U-net: Convolutional networks for biomedical image segmentation. Paper presented at: International Conference on Medical Image Computing and Computer-Assisted Intervention; October 5, 2015-October 9, 2015; Munich, Germany.

15. Zaidi SSA, Ansari MS, Aslam A, Kanwal N, Asghar M, Lee B. A survey of modern deep learning based object detection models. *Digit Signal Process*. 2022;126:103514.

16. Zhao Z-Q, Zheng P, Xu S-t, Wu X. Object detection with deep learning: a review. *IEEE Trans Neural Netw Learn Syst*. 2019;30:3212–3232.

17. Girshick R, Donahue J, Darrell T, Malik J. Rich feature hierarchies for accurate object detection and semantic segmentation. Paper presented at: Proceedings of the IEEE conference on computer vision and pattern recognition; June 24, 2014-June 27, 2014; Columbus, OH.

18. Girshick R. Fast R-CNN. Paper presented at: Proceedings of the IEEE International Conference on Computer Vision; December 11, 2015-December 18, 2015; Santiago, Chile.

19. Ren S, He K, Girshick R, Sun J, Faster R-CNN. towards real-time object detection with region proposal networks. *Adv Neural Inf Process Syst*. 2015;1:91–99.

20. He K, Gkioxari G, Dollár P, Girshick R. Mask R-CNN. Paper presented at: Proceedings of the IEEE International Conference on Computer Vision; October 22, 2017-October 29, 2017; Venice, Italy.

21. Redmon J, Divvala S, Girshick R, Farhadi A. You only look once: unified, real-time object detection. Paper presented at: Proceedings of the IEEE Conference on Computer Vision and Pattern Recognition; June 26, 2016-July 1, 2016; Las Vegas, NV.

22. Redmon J, Farhadi A. YOLO9000: better, faster, stronger. Paper presented at: Proceedings of the IEEE Conference on Computer Vision and Pattern Recognition; July 21, 2017-July 26, 2017; Honolulu, HI.

23. Zhu J-Y, Park T, Isola P, Efros AA. Unpaired image-to-image translation using cycle-consistent adversarial networks. Paper presented at: Proceedings of the IEEE International Conference on Computer Vision; October 22, 2017-October 29, 2017; Venice, Italy.

24. Wang Z, Bovik AC, Sheikh HR, Simoncelli EP. Image quality assessment: from error visibility to structural similarity. *IEEE Trans Image Process*. 2004;13:600–612.

25. Küstner T, Munoz C, Psenicny A, et al. Deep-learning based super-resolution for 3D isotropic coronary MR angiography in less than a minute. *Magn Reson Med*. 2021;86:2837–2852.

26. Liu P, Wang M, Wang Y, et al. Impact of deep learning-based optimization algorithm on image quality of low-dose coronary CT angiography with noise reduction: a prospective study. *Acad Radiol*. 2020;27:1241–1248.

27. Tatsugami F, Higaki T, Nakamura Y, et al. Deep learning-based image restoration algorithm for coronary CT angiography. *Eur Radiol*. 2019;29:5322–5329.

28. Chen H, Zhang Y, Zhang W, et al. Low-dose CT via convolutional neural network. *Biomed Opt Express*. 2017;8:679–694.

29. Benz DC, Ersözlü S, Mojon FL, et al. Radiation dose reduction with deep-learning image reconstruction for coronary computed tomography angiography. *Eur Radiol*. 2022;32:2620–2628.

30. Benz DC, Benetos G, Rampidis G, et al. Validation of deep-learning image reconstruction for coronary computed tomography angiography: impact on noise, image quality and diagnostic accuracy. *J Cardiovasc Comput Tomogr*. 2020;14:444–451.

31. Chu M, Cortés C, Liu L, et al. Comprehensive appraisal of cardiac motion artefact in optical coherence tomography. *Cardiol J*. Published online October 28, 2021. https://doi.org/10.5603/CJ.a2021.0137

32. Stevens TS, Chennakeshava N, de Bruijn FJ, Pekař M, van Sloun RJ. Accelerated intravascular ultrasound imaging using deep reinforcement learning. Paper presented at: ICASSP 2022-2022 IEEE International Conference on Acoustics, Speech and Signal Processing (ICASSP); May 2022; Singapore.

33. Erdogan E, Huang X, Cooper J, et al. End-diastolic segmentation of intravascular ultrasound images enables more reproducible volumetric analysis of atheroma burden. *Catheter Cardiovasc Interv*. 2022;99:706–713.

34. Liang D, Wang L, Han D, et al. Semi 3D-TENet: semi 3D network based on temporal information extraction for coronary artery segmentation from angiography video. *Biomed Signal Process Control*. 2021;69:102894.

35. Du T, Xie L, Zhang H, et al. Training and validation of a deep learning architecture for the automatic analysis of coronary angiography. *EuroIntervention*. 2021;17:32–40.

36. Erlinge D, Maehara A, Ben-Yehuda O, et al. Identification of vulnerable plaques and patients by intracoronary near-infrared spectroscopy and ultrasound (PROSPECT II): a prospective natural history study. *Lancet*. 2021;397:985–995.

37. Kedhi E, Berta B, Roleder T, et al. Thin-cap fibroatheroma predicts clinical events in diabetic patients with normal fractional flow reserve: the COMBINE OCT–FFR trial. *Eur Heart J*. 2021;42:4671–4679.

38. Prati F, Romagnoli E, Gatto L, et al. Relationship between coronary plaque morphology of the left anterior descending artery and 12 months clinical outcome: the CLIMA study. *Eur Heart J*. 2019;41:383–391.

39. Lin A, Manral N, McElhinney P, et al. Deep learning-enabled coronary CT angiography for plaque and stenosis quantification and cardiac risk prediction: an international multicentre study. *Lancet Digit Health*. 2022;4:e256–e265.

40. Al'Aref SJ, Singh G, Choi JW, et al. A boosted ensemble algorithm for determination of plaque stability in high-risk patients on coronary CTA. *J Am Coll Cardiol Img*. 2020;13:2162–2173.

41. Han D, Kolli KK, Al'Aref SJ, et al. Machine learning framework to identify individuals at risk of rapid progression of coronary atherosclerosis: from the PARADIGM registry. *J Am Heart Assoc*. 2020;9:e013958.

42. Eisenberg E, McElhinney PA, Commandeur F, et al. Deep learning-based quantification of epicardial adipose tissue volume and attenuation predicts major adverse cardiovascular events in asymptomatic subjects. *Circ Cardiovasc Imaging*. 2020;13:e009829.

43. Oikonomou EK, Williams MC, Kotanidis CP, et al. A novel machine learning-derived radiotranscriptomic signature of perivascular fat improves cardiac risk prediction using coronary CT angiography. *Eur Heart J*. 2019;40:3529–3543.

44. Knuuti J, Revenco V. 2019 ESC guidelines for the diagnosis and management of chronic coronary syndromes. *Eur Heart J*. 2020;41:407–477.

45. SCOT-HEART Investigators, Newby DE, Adamson PD, et al. Coronary CT angiography and 5-year risk of myocardial infarction. *N Engl J Med*. 2018;379:924–933.

46. Mintz GS, Guagliumi G. Intravascular imaging in coronary artery disease. *Lancet*. 2017;390:793–809.

47. Chu M, Jia H, Gutiérrez-Chico JL, et al. Artificial intelligence and optical coherence tomography for the automatic characterisation of human atherosclerotic plaques. *EuroIntervention*. 2021;17:41–50.

48. Hong H, Jia H, Zeng M, et al. Risk stratification in acute coronary syndrome by comprehensive morphofunctional assessment with optical coherence tomography. *JACC: Asia*. 2022;2(4):460–472.

49. Neumann F-J, Sousa-Uva M, Ahlsson A, et al. 2018 ESC/EACTS guidelines on myocardial revascularization. *Eur Heart J*. 2019;40:87–165.

50. Bech GJW, De Bruyne B, Pijls NH, et al. Fractional flow reserve to determine the appropriateness of angioplasty in moderate coronary stenosis: a randomized trial. *Circulation*. 2001;103:2928–2934.

51. Tonino PA, De Bruyne B, Pijls NH, et al. Fractional flow reserve versus angiography for guiding percutaneous coronary intervention. *N Engl J Med*. 2009;360:213–224.

52. De Bruyne B, Pijls NH, Kalesan B, et al. Fractional flow reserve-guided PCI versus medical therapy in stable coronary disease. *N Engl J Med*. 2012;367:991–1001.

53. Lee HS, Lee JM, Nam C-W, et al. Consensus document for invasive coronary physiologic assessment in Asia-Pacific countries. *Cardiol J*. 2019;26:215–225.

54. Götberg M, Christiansen EH, Gudmundsdottir IJ, et al. Instantaneous wave-free ratio versus fractional flow reserve to guide PCI. *N Engl J Med*. 2017;376:1813–1823.

55. Svanerud J, Ahn JM, Jeremias A, et al. Validation of a novel non-hyperaemic index of coronary artery stenosis severity: the Resting Full-cycle Ratio (VALIDATE RFR) study. *EuroIntervention*. 2018;14:806–814.

56. Tu S, Westra J, Yang J, et al. Diagnostic accuracy of fast computational approaches to derive fractional flow reserve from diagnostic coronary angiography: the international multicenter FAVOR pilot study. *J Am Coll Cardiol Intv*. 2016;9:2024–2035.

57. Xu B, Tu S, Qiao S, et al. Diagnostic accuracy of angiography-based quantitative flow ratio measurements for online assessment of coronary stenosis. *J Am Coll Cardiol*. 2017;70:3077–3087.

58. Itu L, Rapaka S, Passerini T, et al. A machine-learning approach for computation of fractional flow reserve from coronary computed tomography. *J Appl Physiol*. 2016;121:42–52.

59. Coenen A, Kim Y-H, Kruk M, et al. Diagnostic accuracy of a machine-learning approach to coronary computed tomographic angiography-based fractional flow reserve: result from the MACHINE consortium. *Circ Cardiovasc Imaging*. 2018;11:e007217.

60. Tu S, Ding D, Chang Y, Li C, Wijns W, Xu B. Diagnostic accuracy of quantitative flow ratio for assessment of coronary stenosis significance from a single angiographic view: a novel method based on bifurcation fractal law. *Catheter Cardiovasc Interv*. 2021;97:1040–1047.

61. Ding D, Tu S, Chang Y, Li C, Xu B, Wijns W. Quantitative flow ratio based on Murray fractal law: accuracy of single versus two angiographic views. *J Soc Cardiovasc Angiogr Interv*. 2022;1(5):100399.

62. Cortés C, Liu L, Berdin SL, et al. Agreement between Murray law-based quantitative flow ratio (uQFR) and three-dimensional quantitative flow ratio (3D-QFR) in non-selected angiographic stenosis: a multicenter study. *Cardiol J*. 2022;29(3):388–395.

63. Yu W, Tanigaki T, Ding D, et al. Accuracy of intravascular ultrasound-based fractional flow reserve in identifying hemodynamic significance of coronary stenosis. *Circ Cardiovasc Interv*. 2021;14:e009840.

64. Gutiérrez-Chico JL, Chen Y, Yu W, et al. Diagnostic accuracy and reproducibility of optical flow ratio for functional evaluation of coronary stenosis in a prospective series. *Cardiol J*. 2020;27:350–361.

65. Yu W, Huang J, Jia D, et al. Diagnostic accuracy of intracoronary optical coherence tomography-derived fractional flow reserve for assessment of coronary stenosis severity. *EuroIntervention*. 2019;15:189.

66. Piayda K, Kleinebrecht L, Afzal S, et al. Dynamic coronary roadmapping during percutaneous coronary intervention: a feasibility study. *Eur J Med Res*. 2018;23:36.

67. Yabe T, Muramatsu T, Tsukahara R, et al. The impact of percutaneous coronary intervention using the novel dynamic coronary roadmap system. *J Am Coll Cardiol*. 2018;71. A1103-A1103.

68. Ma H, Smal I, Daemen J, Walsum TV. Dynamic coronary roadmapping via catheter tip tracking in X-ray fluoroscopy with deep learning based Bayesian filtering. *Med Image Anal*. 2020;61:101634.

69. Jeong D, Kim D, Ryu J, Cho KH. Deep-learning-based registration of diagnostic angiogram and live fluoroscopy for percutaneous coronary intervention. *IEEE Access*. 2021;9:103465–103480.

70. Wu W, Zhang J, Peng W, Xie H, Zhang S, Gu L. CAR-Net: a deep learning-based deformation model for 3D/2D coronary artery registration. *IEEE Trans Med Imaging*. 2022;41(10):2715–2727.

71. Wu P, Gutiérrez-Chico JL, Tauzin H, et al. Automatic stent reconstruction in optical coherence tomography based on a deep convolutional model. *Biomed Opt Express*. 2020;11:3374–3394.

72. Cortes C, Chu M, Schincariol M, et al. Identification of the type of stent with three-dimensional optical coherence tomography: the SPQR study. *EuroIntervention*. 2020;17(2):e140–e148.

73. Min H-S, Ryu D, Kang S-J, et al. Prediction of coronary stent underexpansion by pre-procedural intravascular ultrasound-based deep learning. *J Am Coll Cardiol Intv*. 2021;14:1021–1029.

74. Antoniades C, Oikonomou EK. Artificial intelligence in cardiovascular imaging—principles, expectations, and limitations. *Eur Heart J*. Published online September 24, 2021. https://doi.org/10.1093/eurheartj/ehab678

75. Fuin N, Bustin A, Küstner T, et al. A multi-scale variational neural network for accelerating motion-compensated whole-heart 3D coronary MR angiography. *Magn Reson Imaging*. 2020;70:155–167.

76. Qi H, Hajhosseiny R, Cruz G, et al. End-to-end deep learning nonrigid motion-corrected reconstruction for highly accelerated free-breathing coronary MRA. *Magn Reson Med*. 2021;86:1983–1996.

77. Azizmohammadi F, Navarro Castellanos I, Miró J, Segars P, Samei E, Duong L. Generative learning approach for radiation dose reduction in X-ray guided cardiac interventions. *Med Phys*. 2022;49(6):4071–4081.

78. Jung S, Lee S, Jeon B, Jang Y, Chang H-J. Deep learning cross-phase style transfer for motion artifact correction in coronary computed tomography angiography. *IEEE Access*. 2020;8:81849–81863.

79. Deng F, Wan Q, Zeng Y, et al. Image restoration of motion artifacts in cardiac arteries and vessels based on a generative adversarial network. *Quant Imaging Med Surg*. 2022;12:2755.

80. Xia M, Yang H, Huang Y, et al. AwCPM-Net: a collaborative constraint GAN for 3D coronary artery reconstruction in intravascular ultrasound sequences. *IEEE J Biomed Health Inform*. 2022;26(7):3047–3058.

81. Bajaj R, Huang X, Kilic Y, et al. A deep learning methodology for the automated detection of end-diastolic frames in intravascular ultrasound images. *Int J Cardiovasc Imaging*. 2021;37:1825–1837.

82. Zhao C, Vij A, Malhotra S, et al. Automatic extraction and stenosis evaluation of coronary arteries in invasive coronary angiograms. *Comput Biol Med*. 2021;136:104667.

83. Pang K, Ai D, Fang H, Fan J, Song H, Yang J. Stenosis-DetNet: sequence consistency-based stenosis detection for X-ray coronary angiography. *Comput Med Imaging Graph*. 2021;89:101900.

84. Li Y, Wu Y, He J, et al. Automatic coronary artery segmentation and diagnosis of stenosis by deep learning based on computed tomographic coronary angiography. *Eur Radiol*. 2022;32(9):6037–6045.

85. Ma X, Luo G, Wang W, Wang K. Transformer network for significant stenosis detection in CCTA of coronary arteries. Paper presented at: International Conference on Medical Image Computing and Computer-Assisted Intervention; September 27, 2021-October 1, 2021; Strasbourg, France.

86. Wang Z-Q, Zhou Y-J, Zhao Y-X, et al. Diagnostic accuracy of a deep learning approach to calculate FFR from coronary CT angiography. *J Geriatr Cardiol*. 2019;16:42.

87. Kumamaru KK, Fujimoto S, Otsuka Y, et al. Diagnostic accuracy of 3D deep-learning-based fully automated estimation of patient-level minimum fractional flow reserve from coronary computed tomography angiography. *Eur Heart J Cardiovasc Imaging*. 2020;21:437–445.

88. Zreik M, Van Hamersvelt RW, Wolterink JM, Leiner T, Viergever MA, Išgum I. A recurrent CNN for automatic detection and classification of coronary artery plaque and stenosis in coronary CT angiography. *IEEE Trans Med Imaging*. 2018;38:1588–1598.

89. Wolterink JM, Leiner T, de Vos BD, van Hamersvelt RW, Viergever MA, Išgum I. Automatic coronary artery calcium scoring in cardiac CT angiography using paired convolutional neural networks. *Med Image Anal*. 2016;34:123–136.

90. Du H, Ling L, Yu W, et al. Convolutional networks for the segmentation of intravascular ultrasound images: evaluation on a multicenter dataset. *Comput Methods Programs Biomed*. 2022;215:106599.

91. Jun TJ, Kang S-J, Lee J-G, et al. Automated detection of vulnerable plaque in intravascular

ultrasound images. *Med Biol Eng Comput*. 2019;57:863–876.

92. Moon JH, Cha WC, Chung MJ, Lee K-S, Cho BH, Choi JH. Automatic stenosis recognition from coronary angiography using convolutional neural networks. *Comput Methods Programs Biomed*. 2021;198:105819.

93. Zreik M, Lessmann N, van Hamersvelt RW, et al. Deep learning analysis of the myocardium in coronary CT angiography for identification of patients with functionally significant coronary artery stenosis. *Med Image Anal*. 2018;44:72–85.

94. Tamarappoo BK, Lin A, Commandeur F, et al. Machine learning integration of circulating and imaging biomarkers for explainable patient-specific prediction of cardiac events: a prospective study. *Atherosclerosis*. 2021;318:76–82.

95. Commandeur F, Slomka PJ, Goeller M, et al. Machine learning to predict the long-term risk of myocardial infarction and cardiac death based on clinical risk, coronary calcium, and epicardial adipose tissue: a prospective study. *Cardiovasc Res*. 2020;116:2216–2225.

96. Kwan AC, McElhinney PA, Tamarappoo BK, et al. Prediction of revascularization by coronary CT angiography using a machine learning ischemia risk score. *Eur Radiol*. 2021;31:1227–1235.

97. Neleman T, Liu S, Tovar Forero MN, et al. The prognostic value of a validated and automated intravascular ultrasound-derived calcium score. *J Cardiovasc Transl Res*. 2021;14:992–1000.

98. Fang H, Li H, Song S, et al. Motion-flow-guided recurrent network for respiratory signal estimation of x-ray angiographic image sequences. *Phys Med Biol*. 2020;65:245020.

99. Kweon J, Kim K, Lee C, et al. Deep reinforcement learning for guidewire navigation in coronary artery phantom. *IEEE Access*. 2021;9:166409–166422.

100. Sayadi A, Nourani HR, Jolaei M, Dargahi J, Hooshiar A. Force estimation on steerable catheters through learning-from-simulation with ex-vivo validation. Paper presented at: 2021 International Symposium on Medical Robotics (ISMR); November 17, 2021-November 19, 2021; Atlanta, GA.

101. Lu H, Lee J, Jakl M, et al. Application and evaluation of highly automated software for comprehensive stent analysis in intravascular optical coherence tomography. *Sci Rep*. 2020;10:1–13.

102. Wang Z, Jenkins MW, Linderman GC, et al. 3-D stent detection in intravascular OCT using a Bayesian network and graph search. *IEEE Trans Med Imaging*. 2015;34:1549–1561.

103. Wissel T, Riedl KA, Schaefers K et al. Delineation of coronary stents in intravascular ultrasound pullbacks. Paper presented at: Medical Imaging 2021: Image-Guided Procedures, Robotic Interventions, and Modeling; February 14, 2021-February 18, 2021; San Diego, CA.

104. Yang G, Mehanna E, Li C, et al. Stent detection with very thick tissue coverage in intravascular OCT. *Biomed Opt Express*. 2021;12:7500–7516.

105. Nam HS, Kim CS, Lee JJ, Song JW, Kim JW, Yoo H. Automated detection of vessel lumen and stent struts in intravascular optical coherence tomography to evaluate stent apposition and neointimal coverage. *Med Phys*. 2016;43:1662–1675.

106. Lu H, Lee J, Ray S, et al. Automated stent coverage analysis in intravascular OCT (IVOCT) image volumes using a support vector machine and mesh growing. *Biomed Opt Express*. 2019;10:2809–2828.

KEY WORDS artificial intelligence, coronary artery disease, coronary imaging, deep learning

APPENDIX For a supplemental table, please see the online version of this paper.